International Journal of Pharmaceutics 479 (2015) 399–407

Contents lists available at ScienceDirect

International Journal of Pharmaceutics

journal homepage: www.elsevier.com/locate/ijpharm

Pharmaceutical nanotechnology

Paclitaxel-loaded micelles enhance transvascular permeability and retention of nanomedicines in tumors

Fabienne Danhier [a], Pierre Danhier [b], Christophe J. De Saedeleer [c], Anne-Catherine Fruytier [b], Nathalie Schleich [a], Anne des Rieux [a], Pierre Sonveaux [c], Bernard Gallez [b], Véronique Préat [a,*]

[a] Université catholique de Louvain, Louvain Drug Research Institute, Advanced Drug Delivery and Biomaterials, Avenue Mounier, 73, B1 73.12, 1200 Brussels, Belgium
[b] Université catholique de Louvain, Louvain Drug Research Institute, Laboratory of Biomedical Magnetic Resonance, Avenue Mounier, 73, B1 73.08, 1200 Brussels, Belgium
[c] Université catholique de Louvain, Institut de recherche expérimentale et clinique (IREC), Pole of Pharmacology, Avenue Mounier, 53, B1 53.09, 1200 Brussels, Belgium

ARTICLE INFO

Article history:
Received 4 November 2014
Received in revised form 6 January 2015
Accepted 7 January 2015
Available online 8 January 2015

Keywords:
EPR effect
Paclitaxel
Polymeric micelles
Tumor targeting
Nanomedicine
Tumor vasculature

ABSTRACT

Paclitaxel (PTX)-loaded polymeric micelles (M-PTX) have been shown to enhance the blood flow and oxygenation of tumors 24 h after treatment. We hypothesized that these changes in the tumor microenvironment could lead to an enhancement of the EPR (enhanced permeability and retention) effect. M-PTX, administered 24 h before analysis, increased the accumulation of macromolecules, nanoparticles and polymeric micelles in tumors. This increased EPR effect could be linked to normalization of the tumor vasculature and decreased interstitial fluid pressure. M-PTX used as a pre-treatment allowed a more effective delivery of three nanomedicines into tumors: polymeric micelles, liposomes and nanoparticles. These experiments demonstrate an enhanced EPR effect after M-PTX treatment, which lead to better availability and enhanced efficacy of a subsequent treatment with nanomedicines.

1. Introduction

One of the major limitations of the efficacy of conventional chemotherapy is poor entry of anti-cancer drugs into tumors (Heldin et al., 2004; Jain and Stylianopoulos, 2010; Minchinton and Tannock, 2006). Tumor targeting by nanomedicine-based therapeutics has emerged as a promising approach to overcome the lack of specificity of conventional chemotherapeutic agents. The design of these agents is based on anatomical and physiological differences between normal and tumoral tissues. Nanocarriers (20–200 nm in diameter) can extravasate and accumulate within the interstitial space of tumors by transiting through endothelial pores 10 and 1000 nm in diameter. The general absence of functional lymphatic vessels in most tumors contributes to nanocarrier entrapment and retention. This passive phenomenon is termed the "enhanced permeability and retention (EPR) effect" (Maeda et al., 2009).

Paclitaxel (PTX) is a potent anti-cancer chemotherapy widely used for treatment of solid tumors, particularly of the breast and ovary (Singla et al., 2002). PTX promotes the polymerization of tubulin causing cellular death by disrupting the normal tubule dynamics required for mitotic division (Adams et al., 1993). PTX also has broad inhibitory effects on angiogenesis, which include decreasing the proliferation, mobility and cord formation of endothelial cells, as well as *in vivo* angiogenesis and VEGF-induced neovascularization (Belotti et al., 1996; Myoung et al., 2001).

Previously, we developed self-assembling diblock copolymers made up of ε-caprolactone (CL), trimethylene carbonate (TMC) and mme-PEG$_{750}$ (mmePEG$_{750}$-p(CL-*co*-TMC)). These polymeric micelles were shown as safe and effective delivery system for PTX. *In vitro*, the IC$_{50}$ (HeLa cells) at 24 h of Taxol® and PTX-loaded micelles were 17.6 and 10.6 μg/ml, respectively. mmePEG$_{750}$-p(CL-*co*-TMC) copolymers were not cytotoxic (100 mg/ml) (Danhier et al., 2009a). Additionally, mmePEG$_{750}$-p(CL-*co*-TMC) copolymers have been shown biocompatible, non-cytotoxic and non-hemolytic (up to 20% w/v) (Vandermeulen et al., 2006). *In vivo*, these PTX-loaded polymeric micelles (M-PTX) enhanced the maximum tolerated dose (MTD) of PTX compared to Taxol® (the current

* Corresponding author. Tel.: +32 2 7647320; fax: +32 2 7647398.
E-mail address: veronique.preat@uclouvain.be (V. Préat).

http://dx.doi.org/10.1016/j.ijpharm.2015.01.009
0378-5173/

commercialized form of PTX which contains Cremophor® EL) from 13.5 mg/kg to 80 mg/kg after intraperitoneal injection. Unloaded-micelles were shown to be not cytotoxic *in vivo*. Polymeric micelles are known to extravasate from blood vessels into tumors through fenestrations present in the tumor endothelium and to be retained within the tumor tissue by the EPR effect (Danhier et al., 2010; Maeda, 2001). M-PTX have been shown to improve tumor oxygenation 24 h after treatment, thereby causing radiosensitization. This increased tumor pO_2 was explained by both an increased blood flow and an inhibition of cellular O_2 consumption resulting from the anti-tumor activity of PTX (Fig. 1) (Danhier et al., 2012).

New vessel formation in tumors is initiated by an imbalance between pro-angiogenic and anti-angiogenic factors. Anti-angiogenic therapies should destroy the tumor vasculature, thereby depriving the tumor of oxygen and nutrients. However, some anti-angiogenic agents are able to transiently "normalize" the abnormal tumor vasculature. This leads to remodeling of the vasculature which presents a structure that is more similar to normal vessels, and reduced interstitial fluid pressure (IFP). This concept of normalized vessels could suggest that these "normal" vessels could avoid the EPR effect and compromise the delivery of drugs to tumors. Jain resolved this paradox by comparing properties of normal, tumor and normalized vessels. It appeared that normalized vessels remain permeable to large molecules (Jain, 2005). Hence the normalization induces a better delivery of the therapeutic entities, by keeping intact the EPR effect and decreasing the IFP (Fig. 1). Although mostly described in mouse tumor models, several clinical trials have provided evidence of a normalized vasculature in cancer patients treated with anti-angiogenic agents (Heldin et al., 2004; Jain and Stylianopoulos, 2010).

In the present study, we hypothesized that (i) changes in the tumor microenvironment observed 24 h after treatment with M-PTX enhance the EPR effect, allowing a more effective delivery of anti-cancer nanomedicines into tumors; (ii) the underlying mechanism of enhanced permeability could be related to normalization of the tumor vasculature and finally (iii) M-PTX pre-treatment could be used to enhance the therapeutic response to nanomedicines (Fig. 1).

Two tumor models were used for this study: CT26 colon carcinoma was chosen because of its sensitivity to PTX (Yang et al., 2013) and its angiogenic properties (Lyons et al., 2007). The TLT hepatocarcinoma model was chosen because it is a fast-growing hypoxic model that presents intrinsic radio- and chemo-resistance and it has already been used to exploit vascular "normalization" properties of anti-angiogenic drugs (Segers et al., 2006). Enhanced vascular permeability was first assessed *in vivo* by different methods highlighting intratumoral accumulation of various nano-scaled vectors (FITC-dextran, 35 nm; Evans blue complex, 6 nm; iron oxides, 30 nm and [^{3}H]PTX-loaded-micelles, 23 nm). We also evaluated normalization of the tumor vasculature using whole mount staining (CD-31), immunofluorescence (CD-31 and α-SMA) and the measurement of IFP, using the wick-in-needle technique. Finally, we tested if a second injection of various anti-cancer nanomedicines 24 h after M-PTX could enhance the therapeutic response.

2. Methods

2.1. Polymer synthesis and characterization

The mmePEG$_{750}$-p(CL-*co*-TMC) copolymer (Johnson and Johnson Center for Biomaterials and Advanced Technologies, Somerville, NJ, USA) was synthesized by ring-opening polymerization as described previously. Briefly, the reaction was initiated by PEG monomethylether of 750 Da (mmePEG$_{750}$) at a molar monomer/initiator ratio of 13.3/1. ε-Caprolactone and trimethylene carbonate were added at 1:1 molar ratio. The reaction was catalyzed by stannous octoate and was allowed to run for 24 h at 160 °C. The polymer was then devolatilized under vacuum at 90 °C for 48–72 h. The molecular weight and the polydispersity of the diblock polymer were determined by gel permeation chromatography and the monomer ratio in the polymer by NMR spectroscopy (Ould-Ouali et al., 2004).

2.2. Preparation and characterization of micelles loaded with PTX

PTX-loaded micelles (M-PTX) (PTX, Sigma–Aldrich, USA) were prepared as previously described (Danhier et al., 2009a). For the radiolabeled formulation, PTX was replaced by [2,6-benzamido-^{3}H (N)] paclitaxel (Moravek Biochemicals, USA).

The amount of solubilized PTX in mmePEG$_{750}$-p(CL-*co*-TMC) micelles was determined by HPLC as described previously (Danhier et al., 2009a, 2012). The particle size and ζ potential were determined by photon correlation spectroscopy (PCS) and laser Doppler velocimetry, respectively using a nanosizer ZS (Malvern, UK). Results were analyzed by the CONTIN algorithm and the sizes were calculated based on the volume distributions together with polydispersity indices (PDI). Electrophoretic mobilities were converted to ζ potentials using the Smoluchowski's equation.

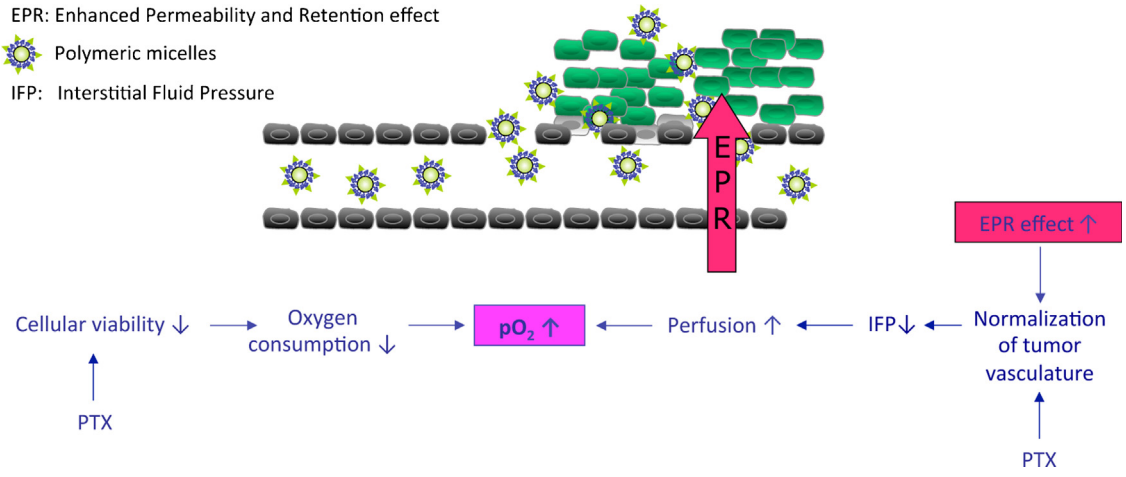

Fig. 1. Schematic representation of the effects of PTX and its influence on the tumoral microenvironment.

2.3. Tumor models

All animal experiments were performed in compliance with the guidelines set by national regulations and were approved by the Ethical Committee for Animal Care of the Université catholique de Louvain (Permit number: UCL/MD/2008/025). All tumor implantation were performed under anesthesia and all efforts were made to minimize suffering.

CT26 colon carcinoma cells (American Type Culture Collection, USA) were grown in DMEM alpha (Gibco® BRL, USA) with 10% (v/v) fetal bovine serum, 100 IU/ml of penicillin G sodium and 100 μg/ml of streptomycin sulfate. Five week-old female Balb/c mice were injected subcutaneously in the right flank with 100 μl of a suspension containing 5×10^4 CT26 cells. Treatments started when the tumor volume reached $27 \pm 5\ mm^3$. Spheroidal–ellipsoidal tumors were measured using an electronic caliper and the volume was calculated using the formula: length × width × height. When individual tumors reached $600\ mm^3$, mice were sacrificed (Schleich et al., 2013; Na et al., 2010).

Hepatocarcinoma TLT tumors were injected intramuscularly into the gastrocnemius muscle of the rear leg of syngeneic 8 week-old male NMRI mice. Before injection, animals were anesthetized with ketamine/xylazine (62.5 and 6.25 mg/kg, respectively). Treatments were applied when the tumors reached 8.0 ± 0.5 mm in diameter. Because of their localization and their non-spheroidal appearance, tumors were measured using an electronic caliper, determining directly the tumor diameter. Mice were sacrificed when the tumors reached 18 mm in diameter (Danhier et al., 2012; Taper et al., 1966).

2.4. Tumor accumulation of various nano-scaled vectors

2.4.1. Accumulation of FITC-dextran: intravital microscopy

Intravital microscopy was performed to allow the visualization of tumor vessels. Preparation of dorsal skin-flap window chambers was adapted from previously described procedures (Sonveaux et al., 2012). Briefly, mice were anesthetized (ketamine/xylazine) and their fur was depilated. A 12-mm circular piece of the superficial back skin was surgically removed together with the upper fascia and centered into a 2-sided titanium frame with a size-matched window. The frame was then sutured. Twenty microliters of CT26 or TLT cell suspension (10^6 cells/ml) was injected between the remaining fascia and skin, and the window was closed with a circular glass coverslip secured with a snap ring. Experiments started 7 days after implantation. The mice were injected intraperitoneally with M-PTX (80 mg/kg); control mice were injected with PBS. Twenty-four hours post-treatment, the mice were anesthetized using 2.5% isoflurane administered via facemask. They were then injected intravenously with FITC-dextran (150 kDa, 50 μl–15 mg/kg, dilution in PBS, Sigma–Aldrich, USA) and images of functional vessels were captured with an AxioCam MRc5 camera (Zeiss, Germany) on a heated Zeiss Axioskop 40 fluorescent microscope. Selected tumor regions were examined using green excitation filters (470–490 nm).

2.4.2. Accumulation of Evans blue complex: Miles assay

The Miles assay (Evans blue technique) was used to measure the tumor vasopermeability to macromolecules. This assay provides a good estimation of the extravasation and interstitial accumulation of macromolecules due to the electrostatic combination of the Evans blue complex (6 nm) with the negatively charged albumin (Miles and Miles, 1952). Briefly, Evans blue (10 mg/kg, dilution in NaCl 0.9%) was administered intravenously in the tail vein of mice 24 h post M-PTX treatment (80 mg/kg) to CT26 or TLT tumor-bearing mice. The dye was allowed to circulate for 1 h before sacrificing the animals. Tumors were excised, weighed and transferred into formamide (2 ml/tumor) for 24 h at 55 °C. Samples were then centrifuged and the Evans blue was extracted. Samples were diluted in ethanol (1:3) and Evans blue concentrations were determined by spectrophotometry at 620 nm.

2.4.3. Biodistribution of iron oxides: electron spin resonance (ESR) spectroscopy

To determine if the M-PTX treatment could be used to enhance the entry and retention of other nanocarriers used for a diagnostic purpose, the biodistribution of ultra-small superparamagnetic iron oxides particles (USPIO) was assessed in CT26 and TLT-tumor bearing mice. USPIO (Molday ION, BioPAL, USA) were chosen because their size was equivalent to nanocarriers (diameter = 30 nm) and because their superparamagnetic properties (diagnosis contrast agent) allow for their quantification by ESR spectroscopy (Radermacher et al., 2009, 2010). When CT26 and TLT tumors reached the appropriate size (as aforementioned), the M-PTX treatment (80 mg/kg) was administered intraperitoneally. Iron oxides were administered by tail vein injection 24 h after treatment at a dose of 7.7 mg Fe/kg (Radermacher et al., 2010). After 30 min, mice were sacrificed; tumors, spleens and livers were excised, freeze-dried and then crushed into a fine powder. The powder was weighed and then placed into the X-band ESR spectrometer cavity (Bruker, EMX, 9.4 GHz) (Parameters available in Supplementary M1) (Radermacher et al., 2010).

2.4.4. Biodistribution of radiolabeled PTX-loaded micelles: scintillation counting

To evaluate whether M-PTX pre-treatment could enhance the entry and retention of PTX administered 24 h after the first treatment M-PTX, the biodistribution of radiolabeled-PTX-loaded micelles was assessed in CT26 and TLT-tumor bearing mice. A 300 μl dose of [^{3}H]PTX-loaded-micelles ([^{3}H]PTX dose = 0.03 mCi/ml (= 0.47 μg/ml)) was injected intraperitoneally to tumor-bearing mice 24 h after intraperitoneal injection of either M-PTX (80 mg/kg) or PBS control. Mice were sacrificed 24 h after the second treatment (Danhier et al., 2009a). Tumors were removed and weighed. One milliliter of Tissue Solubilizer Biolute-S (Serva, Germany) and 1 ml of hydrogen peroxide 35% were added to the tumors and were incubated at room temperature for 3 days. Three milliliters Ultima Gold® scintillation cocktail was added to the samples before quantifying the radioactivity in a scintillation counter (Packard Tricarb 2900 TR, PerkinElmer, USA) (Danhier et al., 2009a).

2.5. Effect on the tumor vasculature

All experiments were performed 24 h after the intraperitoneal injection of the M-PTX pre-treatment (80 mg/kg) into mice-bearing TLT tumors of 8 ± 0.5 mm.

2.5.1. Imaging of the tumor vasculature: whole mount staining (CD-31)

Mice were sacrificed and TLT tumors were excised and stored in 4% paraformaldehyde in PBS. TLT tumors were stained using the whole mount staining method (WMS) as previously described (Ansorena et al., 2013; Kardon, 1998). WMS involves staining small pieces of tissue without sectioning onto slides. TLT tumors were cut transversally into 1 mm thick sections and were stained with an endothelial cells specific antibody (Rat anti mouse CD31, 1:50, BD Pharmingen, BD Biosciences, USA). Alexa®Fluor 568 goat anti-rat IgG secondary antibody (1:500, Life Technologies, USA) was used for the detection of endothelial cells. Following completion of immunofluorescence, the tissues were vitrified as previously described (Kardon, 1998). Each section was imaged (300–500 μm stacks) with a Cell Observer Spinning Disk microscope (Zeiss). Image stacks were merged using AxioVision (Zeiss).

2.5.2. Imaging of the tumor vasculature: immunofluorescence (CD31 and α-SMA)

Mice were sacrificed and TLT tumors were excised and embedded in Tissue-Tek OCT compound (Tissue-Tek Sacura). Sections 5 μm thick were mounted onto charged SuperFrost-plus glass slides and stored at −80 °C until staining. The sections were fixed in ice-cold acetone, rehydrated in PBS and immunostained with rat anti-CD31 antibody (1:50) and rabbit anti-α-SMA antibody (1:100) (GeneTex, USA) in 1% bovine serum albumin (BSA) in PBS for 1 h. Incubation with secondary antibodies Alexa®Fluor 568 goat anti-rat IgG (1:500) and Alexa®Fluor 488 goat anti-rabbit IgG (1:500) was carried out for 30 min at room temperature. Sections were then mounted with DAPI-containing Vectashield. Image acquisition was performed using a MIRAX (Zeiss, Belgium) slide scanner, allowing for the acquisition of entire sections, with 350 nm (blue), 470–490 nm (green) and 515–560 nm (red) excitation filters (Danhier et al., 2009b).

2.5.3. Interstitial fluid pressure measurements

Interstitial fluid pressure (IFP) was measured using a "wick-in-needle" apparatus (Crokart et al., 2013). IPF was monitored 24 h post-treatment using a Stryker pressure monitor system (Stryker, 295-1 Pressure, Stryker Corporation, Kalamazoo, MI) specially designed for measuring tissue fluid pressures. The needle was inserted into the center of the tumor, and 50 μl of saline was injected.

2.6. Efficacy of M-PTX pre-treatment: tumor regrowth delay assay

The therapeutic effect of M-PTX was assessed by the daily measurement of the tumor diameter with an electronic caliper. When TLT tumors reached 8.0 ± 5 mm in diameter or CT26 tumors reached a volume of 27 ± 5 mm^3, mice were randomly assigned to a treatment group. Four groups of five mice were treated as follows: group 1: unloaded micelles; group 2: M-PTX (80 mg/kg) at day 1; group 3: M-PTX (80 mg/kg) at day 1 and M-PTX (80 mg/kg) at day 2 and group 4: M-PTX (160 mg/kg) at day 1. The treatments were injected intraperitoneally. Tumors were then measured daily, using an electronic caliper, until reaching a diameter of 18 mm for TLT tumors or a volume of 600 mm^3 for CT26 tumors, at which time the mice were sacrificed.

The efficacy of M-PTX pre-treatment was also evaluated on TLT tumor-bearing NMRI mice 24 h after injection of two other nanomedicines: the liposomal formulation of doxorubicin, Caelix® (10 mg/kg) and RGD-grafted PLGA-based nanoparticles loaded with PTX (5 mg/kg) (RGD-PTX-NP), previously developed in our lab (Danhier et al., 2009b).

2.7. Statistical analysis

All results are represented as the mean ± standard error of the mean (SEM). Student's *t*-test was used for the Miles assay, biodistribution of iron oxides experiments, biodistribution of radiolabeled PTX-loaded micelles and IFP measurements. Re-growth delays were analyzed using two-way ANOVA and Bonferroni post-hoc test. This analysis was performed on end-point values (last measurements of tumor volume or diameter before sacrifices of mice). $p < 0.05$ was considered to be statistically significant.

3. Results

3.1. Polymer characterization

The chemical composition of the polymers determined by proton NMR was in good agreement with the ratio of the charged monomers: the copolymer contained 49 ± 1 mol% of CL and 49 ± 1 mol% of TMC. The weight-averaged molecular weight (M_w) of mmePEG$_{750}$-p-(CL-*co*-TMC) were 5242 Da (PD = 1.9). The polymer critical micellar concentration was previously determined, using the fluorescent probe method, in the range of 20 μg/ml (0.002%; w/v) (Ould-Ouali et al., 2004). The polymers were liquid at room temperature and formed micelles spontaneously in the presence of aqueous media.

3.2. Characterization of micelles loaded with PTX

Consistent with previously published data (Danhier et al., 2009a, 2012), the solubility of PTX reached 1.80 ± 0.15 mg/ml in formulations containing 10% of mmePEG$_{750}$-p(CL-*co*-TMC). The drug loading of the formulation was 1.8 mg/100 mg polymer. This drug loading should be improved by enhancing the copolymer concentration. Indeed copolymers have been shown biocompatible, non-cytotoxic and non-hemolytic (up to 20% w/v). M-PTX had a size and a zeta (ζ) potential of 23.9 ± 0.4 nm and −2.7 ± 0.4 mV, respectively. Physico-chemical characterization of M-PTX was fully described in previous work (Danhier et al., 2009a).

3.3. M-PTX enhance the vascular permeability and retention of various nano-scaled vectors in tumors

Intravital microscopy was performed to allow the visualization of tumor vessels. A tumor size of 2–3 mm in diameter was reached seven days after tumor implantation in the dorsal skin-flap window chamber (Fig. S1A). Few vessels could be observed. Unlike normal blood vessels around tumors, the newly formed vessels were not well organized. They displayed a tortuous structure and frequent branching (Fig. S1B). FITC-dextran (150 kDA, 35 nm) was administered intravenously to visualize the functionality and permeability of this abnormal tumor vasculature (Pink et al., 2012). As shown in Fig. 2A, extravasation of FITC-dextran was clearly enhanced in tumors treated with M-PTX when compared to untreated tumors, both in TLT and CT26 tumors. These results indicate that M-PTX pre-treatment induces increased vascular permeability to macromolecules.

The Miles assay was used to quantify permeability of tumors to macromolecules (Miles and Miles, 1952). As illustrated in Fig. 2B, the uptake of albumin-Evans blue complexes (6 nm) was enhanced in CT26 tumors pre-treated with M-PTX (0.72 ± 0.02 μg/ml) compared to control tumors (0.38 ± 0.08 μg/ml) ($p < 0.05$). The increase in the uptake of albumin-Evans blue complex by M-PTX-treated TLT tumors (0.7 ± 0.04 μg/g) compared to control tumors (0.48 ± 0.1 μg/g) was also statistically significant ($p < 0.05$). These results are consistent with patent blue staining assessed in a previous study showing an increase in tumor perfusion (Danhier et al., 2012).

The biodistribution of iron oxides (30 nm) in CT26 tumors, TLT tumors, spleen and liver 24 h post M-PTX treatment (80 mg/kg) was measured using X-band ESR spectrometry. Iron oxides were injected at a dose of 7.7 mg Fe/kg and were allowed to circulate for 30 min based on literature (Radermacher et al., 2010) and preliminary studies for optimal detection by ESR spectrometry (data not shown). The accumulation of iron oxides was enhanced by 2.1-fold (2.4 ± 0.5 mg *versus* 5.1 ± 0.6 ng Fe/mg tumor, $p < 0.01$) when tumors were pre-treated with M-PTX for TLT tumors and by 1.95-fold (8.6 ± 2.2 *versus* 16.8 ± 3.2 ng Fe/mg tumor, $p < 0.05$) for CT26 tumors when compared to matched untreated tumors (Fig. 2C). Iron oxide uptake by the spleen was increased after M-PTX pre-treatment ($p < 0.05$ and $p < 0.01$ for TLT-and CT26-bearing mice, respectively) (Fig. 2C). In the liver, the accumulation of iron oxides tended to be higher after the pre-treatment for TLT tumors only ($p > 0.05$).

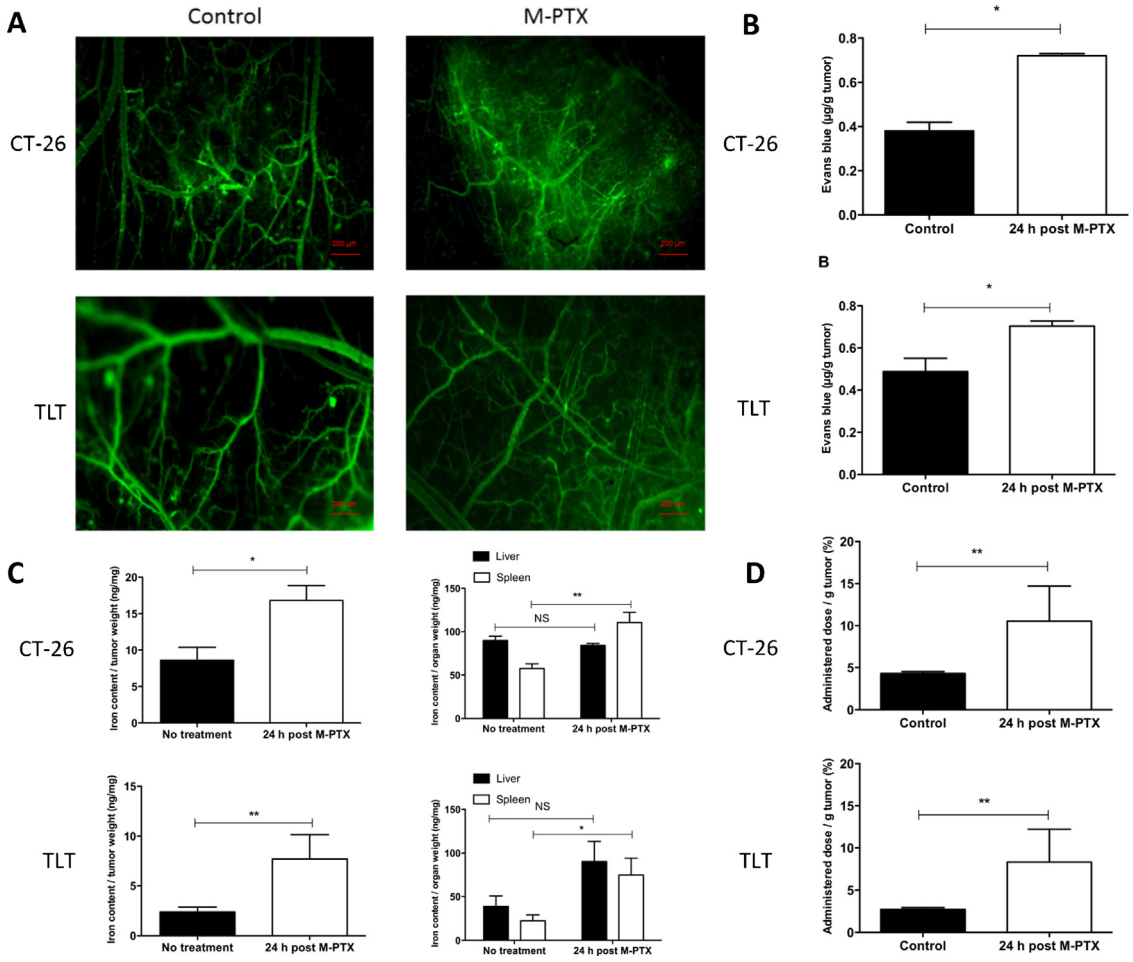

Fig. 2. M-PTX enhance the vascular permeability and retention of various nano-scaled vectors in tumors.
(A) Intravital microscopy images of the extravasation of FITC-dextran (green fluorescence). FITC-dextran was observed in the surrounding tumor tissue, 24 h after M-PTX treatment (80 mg/kg), suggesting the increased permeability of vessels. Extravasation from tumor blood vessels was observed in CT26 and TLT tumors implanted in dorsal skin-flap window chamber-bearing mice (Right). In untreated tumors (Left), no extravasation of FITC-dextran from blood vessels was observed ($n = 4$).
(B) Uptake of albumin-Evans blue complexes in CT26 and TLT tumors-bearing mice 24 h-post M-PTX (80 mg/kg). Data are shown as the means ± SEM ($n = 4$ for CT26 and $n = 3$ for TLT). $^{*}p < 0.05$.
(C) Biodistribution of iron oxides (30 nm) in CT26 and TLT-tumor bearing mice 24 h post-treatment (M-PTX 80 mg/kg). Left: Biodistribution of iron oxides in CT26 or TLT tumors. Right: Biodistribution of iron oxides in the liver and spleen of CT26 or TLT-tumor bearing mice. Data are shown as the means ± SEM ($n = 6$) $^{*}p < 0.05$, $^{**}p < 0.01$.
(D) Biodistribution of [^{3}H]PTX-loaded-micelles in CT26 and TLT-tumor bearing mice 24 h post treatment (M-PTX 80 mg/kg). Data are shown as the means ± SEM ($n = 6$). $^{**}p < 0.01$.

To demonstrate that M-PTX could enhance the dose of PTX that accumulates in tumors by an enhanced EPR effect, the biodistribution of [^{3}H]PTX in CT26 and TLT tumors 24 h post M-PTX treatment (80 mg/kg) was measured using a scintillation counter. The bioavailability of [^{3}H]PTX was enhanced by 2.4-fold (4.3 ± 0.22 *versus* 10.53 ± 4.1% administered dose/g of tumor, $p < 0.01$) when tumors were pre-treated with M-PTX for CT26 tumors, and by 3-fold (2.73 ± 0.51 *versus* 8.3 ± 3.8% administered dose/g of tumor) for TLT tumors ($p < 0.01$) (Fig. 2D). These results demonstrated that pre-treatment of M-PTX allows for improved entry and retention of M-PTX administered as a treatment in tumors.

3.4. M-PTX normalize tumor vasculature and decrease IFP

The architecture of the tumor vasculature was visualized using whole mount staining against CD31 in TLT tumor. As illustrated in Fig. 3A, the tumor vasculature appeared to be better organized and less tortuous when tumors were treated with M-PTX. The normalization window was from 24 h until 5 days after M-PTX treatment (80 mg/kg). The tumor vasculature reverted to a tortuous and disorganized morphology 7 days post-treatment, indicating that the normalization phenomenon had ended.

To confirm the aforementioned observations, immunofluorescence was performed to visualize endothelial cells and pericytes. A unique characteristic of tumor angiogenic vessels is the general lack of a smooth muscle layer and pericytes (Jain, 1987). In contrast, normalized vessels usually present a normal basement membrane and greater coverage by pericytes (Jain, 2005). Consistent with normalization within the expected time frame, many vessels exhibited increased coverage by α-SMA positive cells when tumors were treated with M-PTX compared to untreated tumors (Fig. 3B).

Morphological changes of the normalized tumor vasculature are normally accompanied by functional changes, including increased tumor oxygenation (previously demonstrated with M-PTX (Danhier et al., 2012)) and decreased IFP (which may account for improved penetration of drugs into tumors) (Jain, 2005). IFP was decreased when TLT tumors were pre-treated at 24 h with M-PTX when compared to untreated tumors (10 ± 2.47 *versus* 18.5 ± 4.26 mm Hg, respectively) (Fig. 3C).

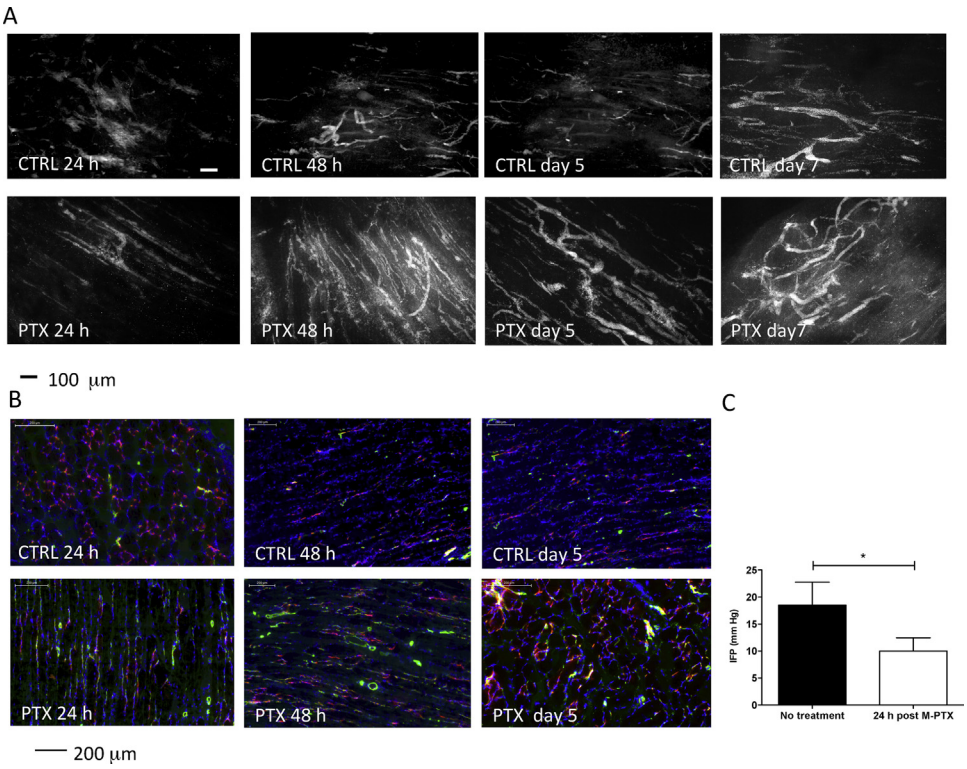

Fig. 3. M-PTX normalize the tumor vasculature in a window of 24 h to day 5 post-treatment. (For interpretation of the references to color in this figure legend, the reader is referred to the web version of this article.)
(A) Confocal microscopy images of the normalization of the TLT tumor vasculature (TLT tumors stained using the Whole Mount Staining method, endothelial cells stained with CD31 specific antibody). The tumor vasculature is better organized 24 h, 48 h and 5 days after M-PTX treatment (80 mg/kg) when compared to untreated tumors, suggesting the normalization of vessels. After 7 days, the vessels appeared to be disorganized ($n = 3$).
(B) Fluorescent microscopy of TLT tumors treated with M-PTX (80 mg/kg) after 24 h, 48 h and 5 days. Sections were stained with anti-CD31 to label endothelial cells (red), anti-α-SMA to label pericytes (green) and counterstained with DAPI to label nuclei (blue) ($n = 3$).
(C) Interstitial fluid pressure (IFP) measurement in TLT 24 h after M-PTX (80 mg/kg) treatment ($n = 6$) or PBS treatment ($n = 6$). Each point represents the means ± SEM. $^{*}p < 0.05$

3.5. M-PTX delay the tumor growth

The *in vivo* anti-tumor efficacy of M-PTX as a pre-treatment to enhance the EPR effect was evaluated in TLT (Fig. 4A) and CT26 tumor-bearing mice (Fig. 4B). M-PTX (80 mg/kg) administered on day 1 and on day 2 displayed higher tumor inhibition than a bolus dose of M-PTX (160 mg/kg) delivered on day 1 ($p < 0.001$ for both tumor types). M-PTX (160 mg/kg) and M-PTX (80 mg/kg at day 1 + day 2) induced a significant delay in regrowth compared to unloaded micelles. Notably, two out of five CT26 tumor-bearing mice died within 2 days of 160 mg/kg M-PTX. This was likely due to the toxicity of the treatment at such high dose, as previously reported (Danhier et al., 2009a).

The *in vivo* anti-tumor efficacy of M-PTX was also evaluated as pre-treatment before the injection of two other nanomedicines: Caelix® (Doxorubicin, 10 mg/kg) (Fig. 4C) and RGD-grafted PLGA based nanoparticles loaded with PTX (RGD-PTX-NP) (PTX, 5 mg/kg) (Fig. 4D).

M-PTX (80 mg/kg) administered 24 h before the injection of both nanomedicines displayed higher tumor inhibition than a single injection of nanomedicine ($p < 0.001$, for Caelix® and RGD-PTX-NP, respectively). This increased delay of regrowth was also observed when compared to the injection of both treatment at day 1 and day 2 ($p < 0.05$ and $p < 0.001$ for Caelix® and RGD-PTX-NP, respectively). In both cases, no loss of body weight was observed (data not shown). M-PTX should therefore be considered as an effective pre-treatment of various types of anti-cancer (PTX and Doxorubicin) nanomedicines (polymeric micelles, liposomes and nanoparticles).

4. Discussion

One of the major causes of failure of conventional chemotherapies is the poor entry of anti-cancer drugs into tumors (Heldin et al., 2004; Jain and Stylianopoulos, 2010; Minchinton and Tannock, 2006). Previously, mmePEG$_{750}$-p(CL-*co*-TMC) polymeric micelles were developed as safe and effective delivery systems for PTX (Danhier et al., 2009a) and have been shown to improve blood flow and oxygenation of tumors 24 h after treatment (Fig. 1) (Danhier et al., 2012). Polymeric micelles may thus be considered to be an innovative tool for administering higher doses of PTX (80 mg/kg). It is important to note that, at this dose of PTX, it was impossible to compare our polymeric micelle formulation with Taxol® due to the death of mice within 2 h when treated with Taxol® at the equivalent PTX dose (Danhier et al., 2012). Moreover, it has been previously demonstrated that unloaded micelles did not present any sign of cytotoxicity both *in vitro* and *in vivo* (Danhier et al., 2009a). In the present study, we hypothesized that increased tumor perfusion could lead to an enhancement of the EPR effect. We demonstrated that the EPR effect was indeed enhanced 24 h after M-PTX treatment, which allowed for a more effective delivery into tumors of three anti-cancer nanomedicines: polymeric micelles loaded with PTX (20 nm, M-PTX), liposomes loaded with doxorubicin (100 nm, Caelix®) and targeted nanoparticles loaded with PTX (230 nm, RGD-PTX-NP).

Using two tumor models and different innovative methods, we showed that M-PTX (80 mg/kg administered 24 h before analysis) was an effective pre-treatment for increasing accumulation of macromolecules and nanoparticles into tumors. Qualitative

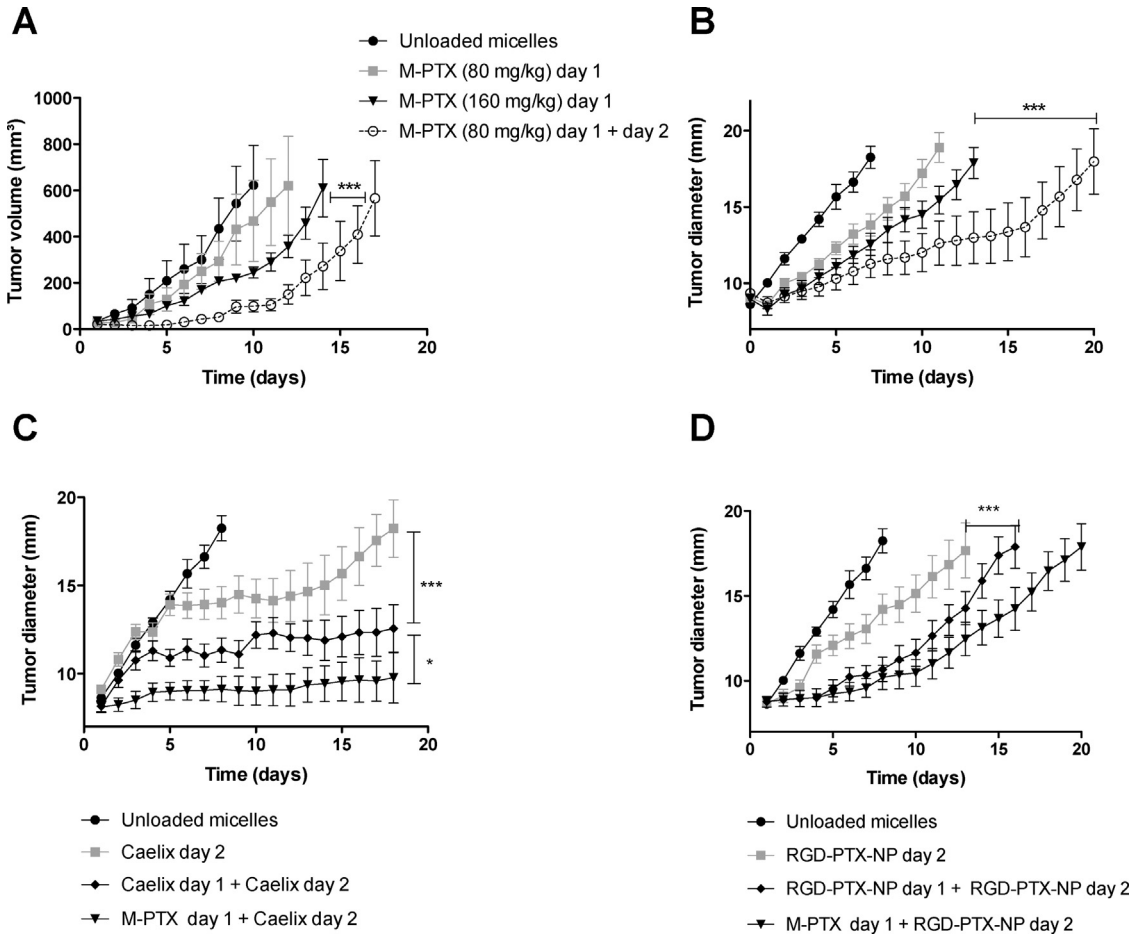

Fig. 4. M-PTX pre-treatment enhance the anti-tumor effect of anti-cancer nanomedicines.
(A) Anti-tumor effect of M-PTX pre-treatment on TLT tumor-bearing mice. Four groups of mice were treated. Group 1: unloaded micelles; group 2: M-PTX (80 mg/kg) at day 1; group 3: M-PTX (80 mg/kg) at day 1 and M-PTX (80 mg/kg) at day 2; group 4: M-PTX (160 mg/kg) at day 1. The treatments were injected intraperitoneally. Data are shown as the mean ± SEM ($n = 5$). $^{***}p < 0.001$.
(B) Anti-tumor effect of M-PTX pre-treatment on CT26 tumor-bearing mice. Four groups of mice were treated. Group 1: unloaded micelles; group 2: M-PTX (80 mg/kg) at day 1; group 3: M-PTX (80 mg/kg) at day 1 and M-PTX (80 mg/kg) at day 2; group 4: M-PTX (160 mg/kg) at day 1. The treatments were injected intraperitoneally. Data are shown as the mean ± SEM. ($n = 5$ for group 1, 2 and 3; $n = 3$ for group 4), $^{***}p < 0.001$.
(C) Anti-tumor effect of Caelix® on TLT tumor-bearing mice. Four groups of mice were treated. Group 1: Unloaded micelles; group 2: Caelix® (DOX 10 mg/kg) at day 2; group 3: M-PTX (80 mg/kg) at day 1 and Caelix® (DOX 10 mg/kg) at day 2; group 4: Caelix® (DOX 10 mg/kg) at day 1 and Caelix® (DOX 10 mg/kg) at day 2. The treatments were injected intraperitoneally. Data are shown as means ± SEM ($n = 6$). $^{*}p < 0.05$, $^{***}p < 0.001$.
(D) Anti-tumor effect of RGD-PTX-NP on TLT tumor-bearing mice. Four groups of mice were treated. Group 1: unloaded micelles; group 2: RGD-PTX-NP (PTX 5 mg/kg) at day 2; group 3: M-PTX (80 mg/kg) at day 1 and RGD-PTX-NP (PTX 5 mg/kg) at day 2; group 4: RGD-PTX-NP (PTX 5 mg/kg) at day 1 and RGD-PTX-NP (PTX 5 mg/kg) at day 2. The treatments were injected intraperitoneally. Data are shown as the mean ± SEM ($n = 6$). $^{***}p < 0.001$.

intravital microscopy using dorsal skin-flap window chambers provided clear evidence of enhanced permeability of the tumor endothelium in M-PTX treated tumors. Specifically, the extravasation of FITC-dextran was drastically enhanced after M-PTX administration compared to untreated tumors. This initial observation was confirmed by three quantitative studies. (i) The Miles assay demonstrated that tumors were more permeable to macromolecules when treated with M-PTX. (ii) ESR spectroscopy showed a higher accumulation of iron oxide particles in tumors, suggesting that M-PTX treatment could be extended to other types of nanomedicines (specifically, nanoparticles used for diagnostic purposes). Accumulation of iron oxides was also enhanced in the spleens and in the livers of mice following M-PTX treatment. To our knowledge, ESR spectroscopy (Radermacher et al., 2009, 2010) has not been used previously for demonstrating an EPR effect. (iii) Enhanced accumulation of radiolabeled-PTX-loaded micelles 24 h after M-PTX treatment clearly demonstrated that M-PTX could be used as a pre-treatment to enhance the entry and accumulation of M-PTX into tumors. Together, these experiments strongly support an enhanced EPR effect after M-PTX pre-treatment (Fig. 2).

We further demonstrated that the underlying mechanism of increased EPR by M-PTX involved vascular normalization occurring in tumors over a time course of 24 h to 5 days after treatment as shown Fig. 3A and B. We previously demonstrated that M-PTX improve tumor oxygenation 24 h after delivery, which we explained by both an increased tumor blood flow in tumors (perfusion) and inhibition of O_2 consumption by cells. The latter was itself linked to a decrease in cell viability due to the anti-tumor effects of PTX (Belotti et al., 1996; Myoung et al., 2001). Indeed, PTX promotes the polymerization of tubulin dimers to form microtubules and then stabilizes the microtubules by preventing depolymerization. Thus, PTX blocks cells in the late G_2 phase and M phase of the cell cycle, inhibiting cell replication. Associated with the phosphorylation of the Bcl-2 protein, cell apoptosis is induced (Adams et al., 1993).

Here, we demonstrated that the enhanced EPR effect is also a direct consequence of decreased IFP (Fig. 3C). In tumors, high

vascular permeability and the absence of functional lymphatic drainage increase the accumulation of plasma proteins in the interstitium, thus increasing IFP by an osmotic effect (Heldin et al., 2004). A clinical study of patients with breast cancer revealed that PTX decreases IFP and improves tumor oxygenation (Taghian et al., 2005). Downregulation of VEGF expression was suggested to be partly responsible for this phenomenon. PTX was found to have broad inhibitory effects on angiogenesis, including the proliferation, motility and cord formation of endothelial cells, the angiogenic response *in vivo* and VEGF-induced neovascularization (Ansiaux et al., 2005). PTX induces a transient normalization of the tumor vasculature and, thus, increased perfusion that accounts for better delivery of chemotherapeutic agents (Segers et al., 2006; Ansiaux et al., 2005; Tong et al., 2004). Other phenomena, such as the compression of blood vessels by proliferating tumor cells in a confined space, can reduce the diameter of blood vessels and, thus, decrease tumor blood flow (Griffon-Etienne et al., 1999). Therefore, the PTX-induced EPR effect in tumors may be the result of (i) enhanced perfusion resulting from a decreased IFP and transient vascular normalization (the anti-angiogenic effect of PTX) and (ii) the decompression of blood vessels resulting from cancer cell death (the cytotoxic effect of PTX).

In the nanoparticles biodistribution study, we observed an increased accumulation of iron oxides in the reticulo-endothelial system (RES): i.e., the spleen and liver. The endothelium of these organs contains fenestrations similar to those found in tumors. Furthermore, iron oxides are known for their preferential accumulation in the RES (Radermacher et al., 2010). Several previous studies have shown that enhancing the availability of chemotherapeutic drugs in tumors is associated with therapeutic benefits (Salnikov et al., 2003). Indeed, drug delivery to tumors is often a limiting step for efficient therapy (Taghian et al., 2005; Tredan et al., 2007). Therefore, strategies to improve the transport of drugs to the tumor should also improve the efficacy of chemotherapy. Another recent study using chorioallantoic membrane (CAM) models indicated that increasing vascular permeability improves the tumor accumulation of doxorubicin (Pink et al., 2012). Therefore, increases in blood flow, permeability and EPR effect that are induced by M-PTX should collectively result in an enhanced accumulation of anti-cancer drugs including nanomedicines (macromolecules or nanoparticles) in tumors. Accordingly, our *in vivo* data demonstrated that a pre-treatment with M-PTX enhances the therapeutic response to various types of anticancer nanomedicines (polymeric micelles, liposomes and nanoparticles) (Fig. 4).

5. Conclusion

In the present study, we report that the pre-treatment M-PTX enhances the EPR effect. The underlying mechanism could be through normalization of the tumor vasculature associated with decreased IFP. This pre-treatment M-PTX leads to enhanced intratumor accumulation and better efficacy of various types of anticancer nanomedicines. M-PTX administration can therefore be considered an effective pre-treatment to improve delivery of an anti-cancer treatment into tumors.

Acknowledgments

This work is supported by grants from the Université catholique de Louvain (F.S.R), *Fonds National de la Recherche Scientifique* (F.R.S.-FNRS), the *Fonds Joseph Maisin*, the Saint-Luc Foundation, the *Fondation contre le Cancer*, the "*Actions de Recherches Concertées-Communauté Française de Belgique*-ARC" (ARC 09/14-020), Interuniversity Attraction Pole (IAP) grant #UP7-03 from the Belgian Science Policy Office (Belspo) and AFCN-FANC grant P.0. 4500020406. P. Sonveaux and A. des Rieux are F.R.S.-FNRS Research Associates, F. Danhier a Postdoctoral F.R.S.-FNRS Research Fellow, and P. Danhier a Research Fellow of the F.R.S.-FNRS. C. J. De Saedeleer is a Télévie Research Fellow. The funders had no role in study design, data collection and analysis, decision to publish, or preparation of the manuscript.

Appendix A. Supplementary data

Supplementary data associated with this article can be found, in the online version, at http://dx.doi.org/10.1016/j.ijpharm.2015.01.009.

References

Adams, J.D., Flora, K.P., Goldspiel, B.R., Wilson, J.W., Arbuck, S.G., et al., 1993. Taxol: a history of pharmaceutical development and current pharmaceutical concerns. J. Natl. Cancer Inst. Monogr. 141–147.
Ansiaux, R., Baudelet, C., Jordan, B.F., Beghein, N., Sonveaux, P., et al., 2005. Thalidomide radiosensitizes tumors through early changes in the tumor microenvironment. Clin. Cancer Res. 11, 743–750.
Ansorena, E., De Berdt, P., Ucakar, B., Simon-Yarza, T., Jacobs, D., et al., 2013. Injectable alginate hydrogel loaded with GDNF promotes functional recovery in a hemisection model of spinal cord injury. Int J. Pharm. 455, 148–158.
Belotti, D., Rieppi, M., Nicoletti, M.I., Casazza, A.M., Fojo, T., et al., 1996. Paclitaxel (Taxol(R)) inhibits motility of paclitaxel-resistant human ovarian carcinoma cells. Clin. Cancer Res. 2, 1725–1730.
Crokart, N., Danhier, F., Daugimont, L., Goncalves, N., Jordan, B.F., et al., 2013. Potentiation of radiotherapy by a localized antiangiogenic gene therapy. Radiother. Oncol. 107, 252–258.
Danhier, F., Magotteaux, N., Ucakar, B., Lecouturier, N., Brewster, M., et al., 2009a. Novel self-assembling PEG-p-(CL-co-TMC) polymeric micelles as safe and effective delivery system for paclitaxel. Eur J. Pharm. Biopharm. 73, 230–238.
Danhier, F., Vroman, B., Lecouturier, N., Crokart, N., Pourcelle, V., et al., 2009b. Targeting of tumor endothelium by RGD-grafted PLGA-nanoparticles loaded with paclitaxel. J. Control. Release 140, 166–173.
Danhier, F., Feron, O., Preat, V., 2010. To exploit the tumor microenvironment: passive and active tumor targeting of nanocarriers for anti-cancer drug delivery. J. Control. Release 148, 135–146.
Danhier, F., Danhier, P., Magotteaux, N., De Preter, G., Ucakar, B., et al., 2012. Electron paramagnetic resonance highlights that the oxygen effect contributes to the radiosensitizing effect of paclitaxel. PLoS One 7, e40772.
Griffon-Etienne, G., Boucher, Y., Brekken, C., Suit, H.D., Jain, R.K., 1999. Taxane-induced apoptosis decompresses blood vessels and lowers interstitial fluid pressure in solid tumors: clinical implications. Cancer Res. 59, 3776–3782.
Heldin, C.H., Rubin, K., Pietras, K., Ostman, A., 2004. High interstitial fluid pressure – an obstacle in cancer therapy. Nat. Rev. Cancer 4, 806–813.
Jain, R.K., Stylianopoulos, T., 2010. Delivering nanomedicine to solid tumors. Nat. Rev. Clin. Oncol. 7, 653–664.
Jain, R.K., 1987. Transport of molecules in the tumor interstitium: a review. Cancer Res. 47, 3039–3051.
Jain, R.K., 2005. Normalization of tumor vasculature: an emerging concept in antiangiogenic therapy. Science 307, 58–62.
Kardon, G., 1998. Muscle and tendon morphogenesis in the avian hind limb. Development 125, 4019–4032.
Lyons, J.A., Sheahan, B.J., Galbraith, S.E., Mehra, R., Atkins, G.J., et al., 2007. Inhibition of angiogenesis by a Semliki Forest virus vector expressing VEGFR-2 reduces tumour growth and metastasis in mice. Gene Ther. 14, 503–513.
Maeda, H., Bharate, G.Y., Daruwalla, J., 2009. Polymeric drugs for efficient tumor-targeted drug delivery based on EPR-effect. Eur. J. Pharm. Biopharm. 71, 409–419.
Maeda, H., 2001. The enhanced permeability and retention (EPR) effect in tumor vasculature: the key role of tumor-selective macromolecular drug targeting. Adv. Enzyme Regul. 41, 189–207.
Miles, A.A., Miles, E.M., 1952. Vascular reactions to histamine, histamine-liberator and leukotaxine in the skin of guinea-pigs. J. Physiol. 118, 228–257.
Minchinton, A.I., Tannock, I.F., 2006. Drug penetration in solid tumours. Nat. Rev. Cancer 6, 583–592.
Myoung, H., Hong, S.D., Kim, Y.Y., Hong, S.P., Kim, M.J., 2001. Evaluation of the anti-tumor and anti-angiogenic effect of paclitaxel and thalidomide on the xenotransplanted oral squamous cell carcinoma. Cancer Lett. 163, 191–200.
Na, H., Lim, Y., Jeong, Y., Lee, H., Lim, Y., et al., 2010. Combination antitumor effects of micelle-loaded anticancer drugs in a CT-26 murine colorectal carcinoma model. Int. J. Pharm. 383, 192–200.
Ould-Ouali, L., Arien, A., Rosenblatt, J., Nathan, A., Twaddle, P., et al., 2004. Biodegradable self-assembling PEG-copolymer as vehicle for poorly water-soluble drugs. Pharm. Res. 21, 1581–1590.
Pink, D.B., Schulte, W., Parseghian, M.H., Zijlstra, A., Lewis, J.D., 2012. Real-time visualization and quantitation of vascular permeability in vivo: implications for drug delivery. PLoS One 7, e33760.
Radermacher, K.A., Beghein, N., Boutry, S., Laurent, S., Vander, E.L., et al., 2009. In vivo detection of inflammation using pegylated iron oxide particles targeted at

E-selectin: a multimodal approach using MR imaging and EPR spectroscopy. Invest. Radiol. 44, 398–404.
Radermacher, K.A., Boutry, S., Laurent, S., Elst, L.V., Mahieu, I., et al., 2010. Iron oxide particles covered with hexapeptides targeted at phosphatidylserine as MR biomarkers of tumor cell death. Contrast Media Mol. Imaging 5, 258–267.
Salnikov, A.V., Iversen, V.V., Koisti, M., Sundberg, C., Johansson, L., et al., 2003. Lowering of tumor interstitial fluid pressure specifically augments efficacy of chemotherapy. FASEB J. 17, 1756–1758.
Schleich, N., Sibret, P., Danhier, P., Ucakar, B., Laurent, S., et al., 2013. Dual anticancer drug/superparamagnetic iron oxide-loaded PLGA-based nanoparticles for cancer therapy and magnetic resonance imaging. Int. J. Pharm. 447, 94–101.
Segers, J., Di, F., Ansiaux, R., Martinive, P., Feron, O., et al., 2006. Potentiation of cyclophosphamide chemotherapy using the anti-angiogenic drug thalidomide: importance of optimal scheduling to exploit the 'normalization' window of the tumor vasculature. Cancer Lett. 244, 129–135.
Singla, A.K., Garg, A., Aggarwal, D., 2002. Paclitaxel and its formulations. Int. J. Pharm. 235, 179–192.
Sonveaux, P., Copetti, T., De Saedeleer, C.J., Vegran, F., Verrax, J., et al., 2012. Targeting the lactate transporter MCT1 in endothelial cells inhibits lactate-induced HIF-1 activation and tumor angiogenesis. PLoS One 7, e33418.
Taghian, A.G., Abi-Raad, R., Assaad, S.I., Casty, A., Ancukiewicz, M., et al., 2005. Paclitaxel decreases the interstitial fluid pressure and improves oxygenation in breast cancers in patients treated with neoadjuvant chemotherapy: clinical implications. J. Clin. Oncol. 23, 1951–1961.
Taper, H.S., Woolley, G.W., Teller, M.N., Lardis, M.P., 1966. A new transplantable mouse liver tumor of spontaneous origin. Cancer Res. 26, 143–148.
Tong, R.T., Boucher, Y., Kozin, S.V., Winkler, F., Hicklin, D.J., et al., 2004. Vascular normalization by vascular endothelial growth factor receptor 2 blockade induces a pressure gradient across the vasculature and improves drug penetration in tumors. Cancer Res. 64, 3731–3736.
Tredan, O., Galmarini, C.M., Patel, K., Tannock, I.F., 2007. Drug resistance and the solid tumor microenvironment. J. Natl. Cancer Inst. 99, 1441–1454.
Vandermeulen, G., Rouxhet, L., Arien, A., Brewster, M., Préat, V., 2006. Encapsulation of amphotericin B in poly(ethylene glycol)-block-poly(epsilon-caprolactone-co-trimethylenecarbonate) polymeric micelles. Int. J. Pharm. 309, 234–240.
Yang, X.Y., Li, Y.X., Li, M., Zhang, L., Feng, L.X., Zhang, N., 2013. Hyaluronic acid-coated nanostructured lipid carriers for targeting paclitaxel to cancer. Cancer Lett. 334, 338–345.